J Appl Electrochem (2014) 44:631–646
DOI 10.1007/s10800-014-0668-0

RESEARCH ARTICLE

Effect of chloride ions on the electrochemical performance of LDX 2003 alloy in concrete and simulated concrete-pore solutions

Omar Rosas · Enrique Maya-Visuet · Homero Castaneda

Received: 20 November 2013 / Accepted: 22 January 2014 / Published online: 8 February 2014

Abstract The aim of this work is to study the effect of chloride ions in the performance of LDX 2003 alloy and to characterize the interface formed in simulated concrete and simulated concrete-pore solutions. In order to have a baseline for analyzing LDX 2003 performance, this alloy is compared with two commonly used materials, AISI 1008 and SAE 316L. Electrochemical techniques such as potentiodynamic scan and electrochemical impedance spectroscopy are used to analyze the qualitative characteristics of the passive layer in four different chloride concentrations for the simulated concrete solutions: 0, 0.05, 0.7, and 3.5 wt%; and four different ratios of $[Cl^-]/[OH^-]$ for the simulated concrete-pore solution: 0, 0.1, 1.0, and 10. For long-term experimental condition, equivalent circuits analogs were applied and the results were analyzed to describe and quantify meaningful parameters for corrosion performance. The electrochemical techniques are complemented by high resolution techniques, such as scanning electron microscopy, atomic force microscopy, and 3D optical microscopy.

Keywords Corrosion · Passive layer · Electrochemical impedance spectroscopy · Scanning electron microscope · Atomic force microscope · 3D optical microscope

1 Introduction

Concrete is the most widely used and produced material on Earth; the use of cement (a key ingredient in concrete) dates back more than 3,500 years [1], and it is still an important material in modern times. In order to improve the mechanical properties of concrete, reinforcing steel (rebar) is used in structures, such as bridges, buildings, highways, tunnels, parking garages, offshore well platforms, and dam walls, among others. The most important feature regarding corrosion resistance is the hydration reaction that occurs between cement and water resulting in a highly alkaline pore solution with a pH between 12.5 and 13.6, under such conditions, reinforced steel tends to form a surface layer with excellent corrosion resistance, however, this passivating layer can be broken down by external factors. The presence of chloride ions can produce a localized breakdown of the passive layer and expose metal to the environmental conditions; chloride ions compete with hydroxide ions needed for the formation of a passivating layer to form instead a soluble, non-stable compound that leads to further dissolution of the metal.

Chloride ions in concrete can originate from either the constituents of the concrete or the surrounding environment. The most common sources of chloride ions are sea water in marine environments and the deicing salts used on road surfaces in cold climates; around 10 million tons of deicing salts are used annually in the United States to lower the freezing point of water and keeping roads safe during winter. There are a number of studies on the effect of chlorides on concrete solution and concrete-pore solution [2–11] trying to identify a critical chloride concentration at which corrosion will occur, but the chloride threshold is still uncertain; values above a threshold of 0.6 for $[Cl^-]/[OH^-]$ ratio in a simulated pore solution were reported to decrease the resistance of the passive film when the pH was below 10 and the iron oxides could not protect the steel substrate from corrosion [5]. One way to face the problem of corrosion due to chlorides is using alternative methods

O. Rosas · E. Maya-Visuet · H. Castaneda (✉)
Department of Chemical and Bio-molecular Engineering, National Center for Education and Research in Corrosion and Materials Performance, The University of Akron, 264 Wolf Ledges Parkway, Akron, OH 44325, USA
e-mail: homeroc@uakron.edu

such as chemical additives or corrosion resistant alloys selection, since the former may increase the cost tenfold [1], the material design approach may be the best solution for decreasing and controlling corrosion of concrete structures.

The use of stainless steel is a popular and effective method for improving the corrosion resistance and durability of the rebar [6]. The high corrosion resistance of stainless steel is due to the presence of a very thin passivating and self-renewing layer composed of a complex oxide film that has a rich chromium oxide/hydroxide inner layer and an iron oxide outer layer [12]; these alloys exhibit a high corrosion resistance in simulated concrete-pore solutions [13]. Although the use of stainless steels may present a real solution for concrete structures in the presence of chlorides, they also present some drawbacks. First, some alloys are susceptible to pitting corrosion in the presence of chlorides [6], and second, in the past few years, there have been strong fluctuations and a net increase in the price of important alloying elements, such as nickel [14]; this fact explains the appearance on the market of new, less-expensive alloys, such as lean-duplex stainless steels. Regardless the protective mechanism, it is undisputed that duplex and lean-duplex steels perform well in alkaline environments in the presence of chlorides [9–11, 14–21].

In the present work, we analyzed the electrochemical performance of the corrosion resistant alloy LDX2003 (UNS S32003) in simulated concrete and simulated concrete-pore solution in the presence of chloride ions; in order to elucidate its behavior, LDX2003 was compared with the electrochemical performance of two materials, C1008 (AISI 1008) and SS 316L (UNS S31603), under the exact same experimental conditions. The electrochemical response was obtained by using impedance spectroscopy (EIS), and a simple electrical analog was carried out to reproduce this signal to aid understanding of the principal mechanisms of passivation and the effect of chloride ions in the passive film. 3D optical microscopy, atomic force microscopy (AFM), and scanning electron microscopy (SEM) coupled to energy-dispersive X-ray spectroscopy (EDS) were used to characterize the surface characteristics.

2 Experimental

2.1 Materials and solutions

The materials tested in the two different electrolytes were LDX 2003 (UNS S32003), carbon steel C1008 (AISI 1008), and SS 316L (UNS S31603). Just before every test, all the materials were polished with up to 1200-grit silicon carbide paper, rinsed, and dried with ethanol. Table 1 shows the compositions of each alloy.

Two different electrolytes were tested; first, a solution simulating the concrete conditions using 2 g L^{-1} of $Ca(OH)_2$, and second, a solution simulating concrete-pore solution using 4.5 g L^{-1} of KOH, 0.8 g L^{-1} NaOH, and 0.8 g L^{-1} $Ca(OH)_2$. Four different concentrations of chloride ions were used for the first system: 0, 0.05, 0.7, and 3.5 wt%. For the second system, four different ratios of $[Cl^-]/[OH^-]$ were used: 0, 0.1, 1.0, and 10, which are equivalent to 0, 0.06, 0.6, and 6.0 wt %. respectively.

2.2 Experimental techniques

All the electrochemical tests were carried out in solutions at 25 °C under controlled atmosphere by a continuous injection of argon gas (99.9 %) at 1 atm. A three-electrode electrochemical cell was used, with the alloy being tested as the working electrode (WE), a saturated calomel electrode as the reference electrode (RE), and a platinum mesh as the counter electrode (CE). The three-electrode arrangement was set up in a water ring cell with an active area of 5 cm^2 to the electrolyte. The tests were carried out using a Solartron™ 1260 potentiostat coupled with a Solartron™ 1287A electrochemical interface.

For the first system, the measuring sequence was open circuit potential (OCP) for 2 h, followed by EIS using an amplitude of ±10 mV and a range of frequencies from 100 kHz to 10 mHz, and finally, a cyclic potentiodynamic curve from the OCP to 1.5 V vs. RE and back to the OCP value; the sweep rate was 1 mV s^{-1}.

For the second system, the measuring sequence was OCP for 2 h, followed by EIS using an amplitude of ±10 mV and a range of frequencies from 100 kHz to 10 mHz, and finally, a cyclic potentiodynamic curve from the OCP to 1.0 V vs. RE and back to the OCP value. For this system, a potentiostatic test was also carried out by applying a potential of 300 mV vs. RE during 96 h, in which EIS was performed every 12 h at the same applied potential.

Following the electrochemical tests, all the samples were dried in an Argon flux to remove the excess solution and they were stored without treating the surface in an oxygen-free environment until taken out for microscopy analysis. The surface morphology and compositional determination of the specimens were carried out by SEM using a HITACHI™ TM3000 Tabletop microscope coupled with EDS and 3D optical microscopy using a Bruker™ Contour GT-I microscope. All the observations were carried out after the electrochemical tests and no surface treatment was given to the samples.

For the simulated concrete solution in the presence of 3.5 wt% NaCl, an atomic force microscope (Multimode 8 Bruker) was used to determine the surface morphology before and after testing. The AFM measurements were performed by using an electrochemical cell (from Bruker),

Table 1 Chemical composition in wt%

Alloy	% C	% Cr	% Mn	% Mo	% Ni	% N	% P	% Si	% S	% Fe
C1008	0.08	NA	0.90	NA	NA	NA	0.04	NA	0.05	Balance
SS 316L	0.03	18.00	2.00	3.0	14.0	0.10	0.045	0.75	0.03	Balance
LDX 2003	0.016	21.59	1.32	1.82	3.80	0.18	0.025	0.32	0.0002	Balance

NA Notation

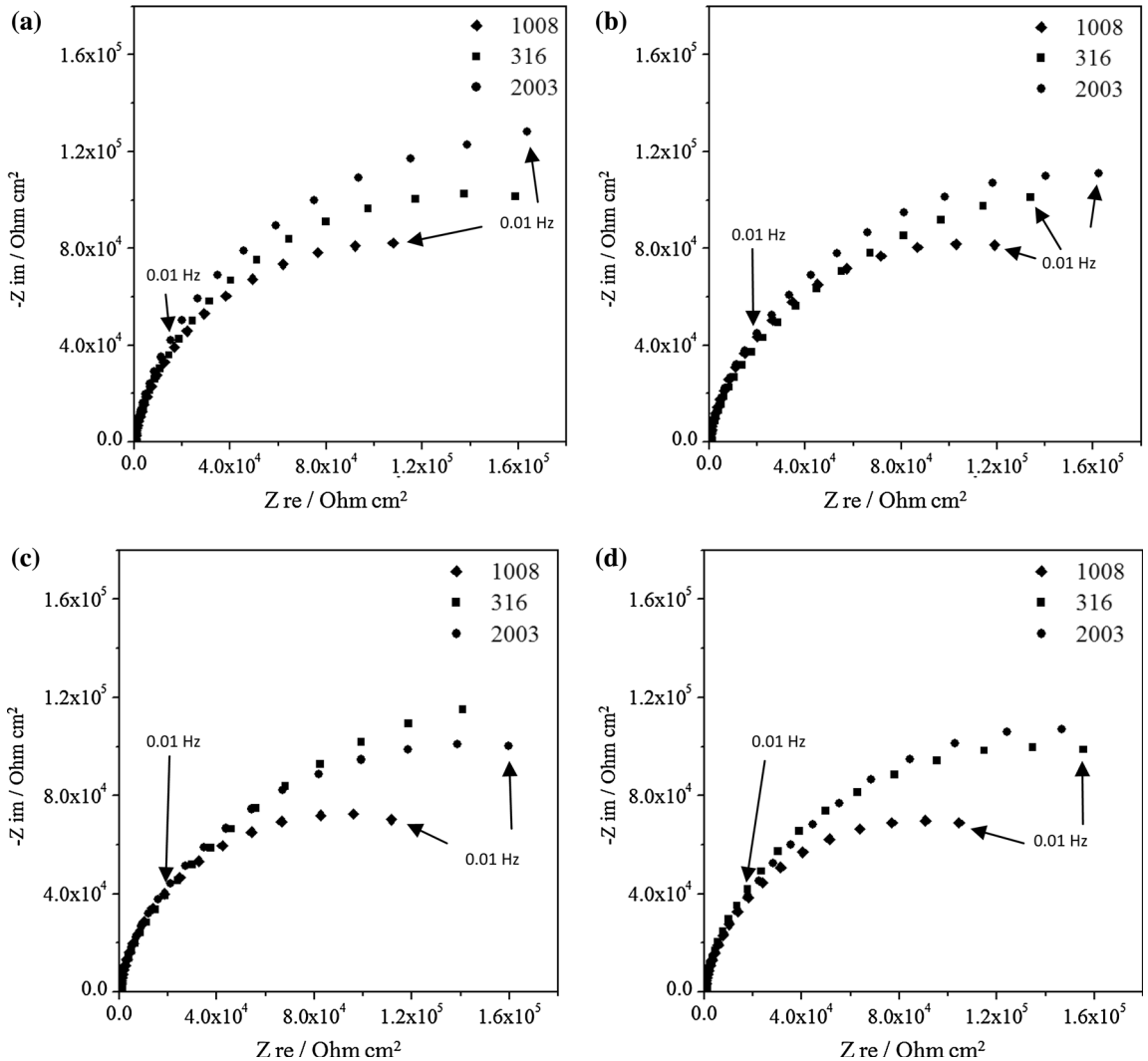

Fig. 1 Nyquist plots for 1,008, 316L, and LDX 2003 in 2 g L^{-1} $Ca(OH)_2$ for **a** 0 wt% NaCl, **b** 0.05 wt% NaCl, **c** 0.7 wt% NaCl, and **d** 3.5 wt% NaCl

the WE was LDX 2003 samples, a platinum mesh electrode was the pseudo-RE, a platinum mesh was the CE, and the electrochemical cell was connected to a GAMRY 600 potentiostat for polarization and EIS testing. The measuring sequence for the AFM electrochemical cell was EIS using an amplitude of ±10 mV and a range of frequencies from 100 kHz to 10 mHz. For this system, a potentiostatic test was also carried out by applying a potential of 300 mV vs. RE during 11 h, in which EIS was performed at the same applied potential.

3 Results and analysis

3.1 Simulated concrete solution

The impedance responses for the three different materials, with increasing chloride concentrations around the OCP, are represented by the Nyquist diagrams shown in Fig. 1.

In Fig. 1, it is observed that the impedance signal around the OCP is very similar for the C1008, SS 316L, and LDX 2003 materials when they were exposed to different

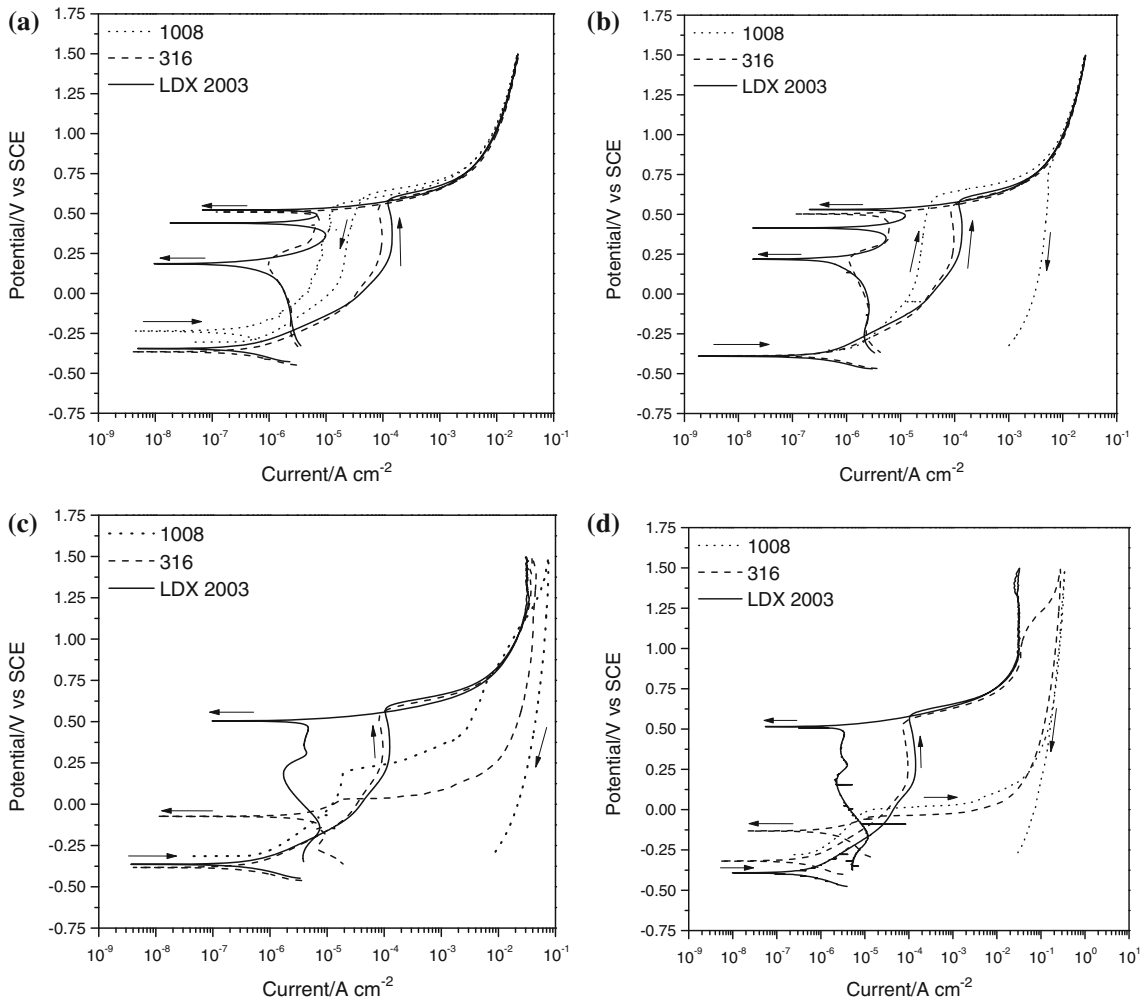

Fig. 2 Potentiodynamic plots for 1,008, 316L, and LDX 2003 in 2 g L^{-1} $Ca(OH)_2$ for **a** 0 wt% NaCl, **b** 0.05 wt% NaCl, and **c** 0.7 wt% NaCl, **d** 316L and LDX 2003 in 2 g L^{-1} $Ca(OH)_2$ in 3.5 wt% NaCl. All the sweep rates were 1 mV s^{-1}

chlorides concentrations. The effect of chlorides is only visible in the highest concentration, where the diameter of the semicircle for the C1008 low-carbon steel is smaller than that of the other materials and smaller than that for the same material but with less-concentrated solutions. However, the mechanisms and magnitude of the impedance are the same. This behavior is due to a similar oxide layer formed in anoxic conditions; the chromium-based passive layer had not yet formed in the stainless steel, and the high pH prevented the low frequencies from reaching the real-impedance axis.

Although the impedance signal for all the materials in all conditions was very close at the OCP, the potentiodynamic curves had completely different behavior, as shown in Fig. 2.

As it can be observed in Fig. 2, in the absence of chlorides, low-carbon steel shows a wider passivation range and lower currents compared to SS 316L and LDX 2003, but most importantly, since the curve shows negative hysteresis, the repassivation potential (E_{rep}) showed no likelihood of pitting corrosion. When increasing the chloride concentration to 0.05 wt%, the SS 316L and LDX 2003 alloys showed the same behavior as in the absence of chlorides, but in this case, C1008 steel showed positive hysteresis and a very low E_{rep}, which indicates a high likelihood of pitting corrosion [22]. When increasing the chloride concentration to 0.7 wt%, low-carbon steel again showed low E_{rep}, and the SS 316L alloy showed positive hysteresis, indicating the likelihood of forming pits, which were found in the SEM and 3D optical microscopy images of Figs. 3 and 4. The LDX 2003 alloy still showed a negative hysteresis and no change in E_{rep}. At 3.5 wt% chlorides, the SS 316L alloy showed an even lower E_{rep} than with the previous chloride concentration, and again, the LDX 2003 alloy showed negative hysteresis and no change in E_{rep}, which is an indication that this alloy will resist the formation of pits under the simulated conditions, as can be seen in the 3D microscopy profile in Fig. 5.

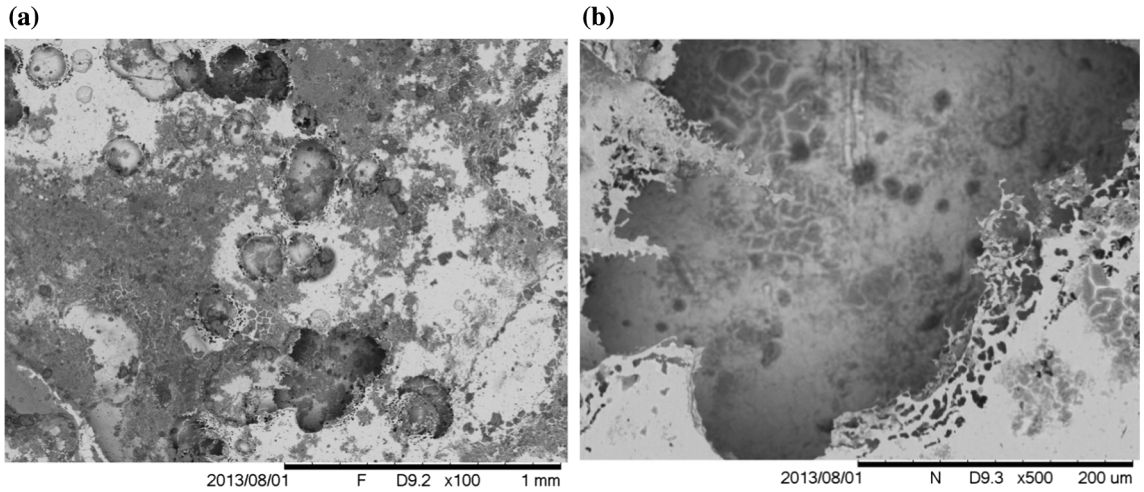

Fig. 3 SEM images of the 316L allow in simulated concrete solution exposed to 0.7 wt% NaCl showing the large pits formed on the surface (nearly 0.2 mm diameter): **a** ×100, and **b** ×500

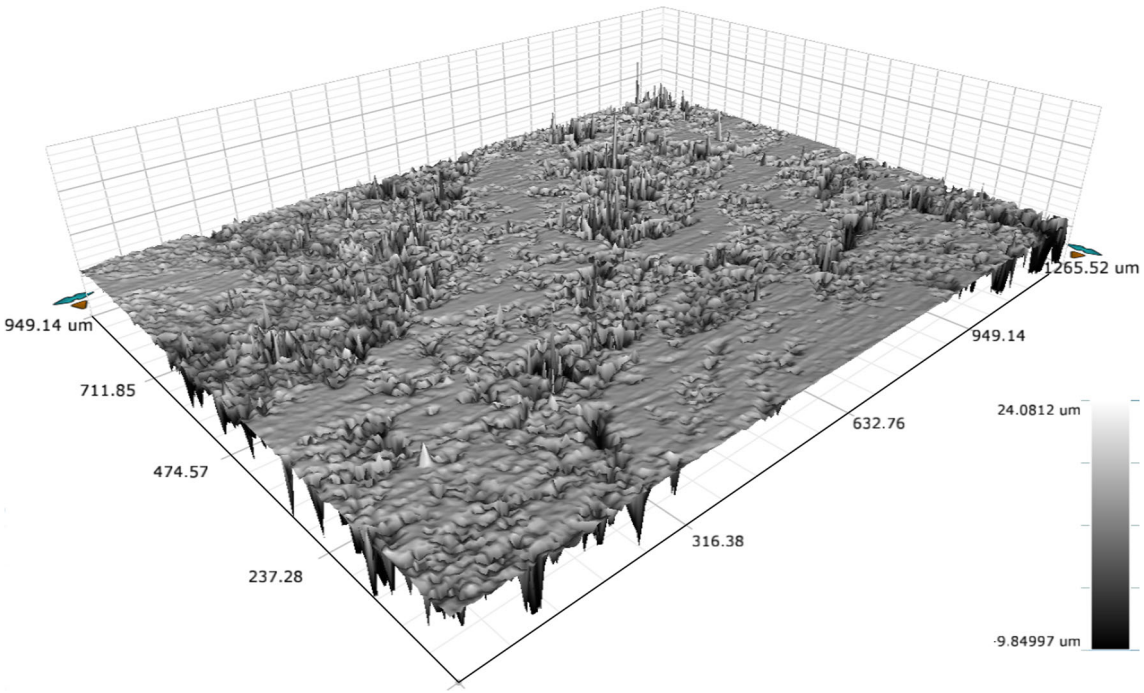

Fig. 4 3D Optical microscopy of the 316L alloy in simulated concrete solution exposed to 0.7 wt% NaCl; the depth of the deepest pit is nearly 10 μm

Table 2 shows the corrosion parameters obtained from the potentiodynamic experiments in the concrete simulated solution. As it is observed, E_{corr} is very similar for all the materials in the different chloride concentrations, J_{corr} and V_{corr} are also quite similar being slightly higher in the low-carbon steel; these parameters do not show any pattern regarding material or concentration, however, pitting potential (E_{pit}) and E_{rep} behave differently. E_{pit} and E_{rep} for carbon steel are strongly dependent upon the chloride concentration; E_{pit} decreases with the increase in chlorides and indicating the likelihood for this material to form pitting corrosion on these conditions, E_{rep} crosses the potentiodynamic curve below E_{corr}, indicating the likelihood for this material to suffer pitting corrosion even at OCP conditions. For SS 316L, E_{pit} remains constant and it is not affected by the concentration of chlorides, however, E_{rep} drops 550 mV from E_{pit} with a positive hysteresis for the cases of 0.7 and 3.5 wt% NaCl, indicating the likelihood of

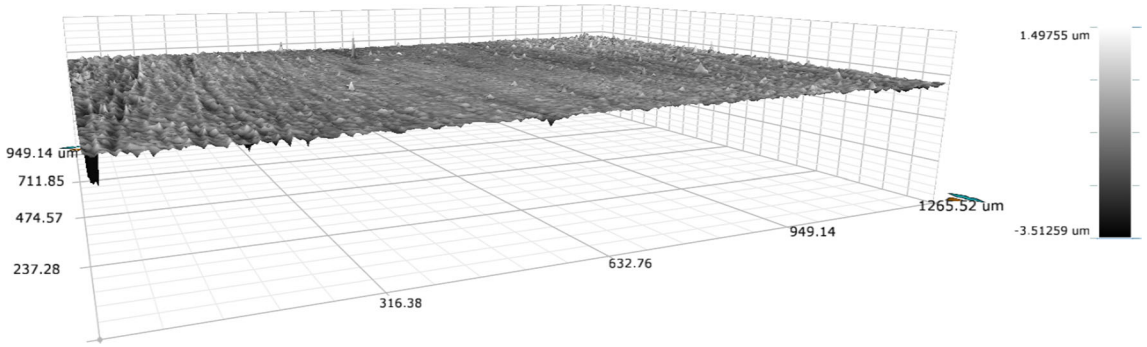

Fig. 5 3D Optical microscopy of the LDX 2003 alloy in simulated concrete solution exposed to 3.5 wt% NaCl; no pits were found on the surface

Table 2 Corrosion parameters for concrete simulated conditions

Alloy	NaCl (wt%)	E_{corr} ($V_{vs\ SCE}$)	J_{corr} (A cm^{-2})	V_{corr} (mm y^{-1})	E_{pit} (V_{vsSCE})	E_{rep} (V_{vsSCE})
C1008	0	−0.24	9.00E−07	0.0105	0.60	0.60
	0.05	−0.35	1.50E−06	0.0174	0.60	–
	0.70	−0.30	8.00E−07	0.0093	0.20	–
	3.50	−0.30	8.00E−07	0.0093	0.05	–
SS 316L	0	−0.34	7.00E−07	0.0080	0.60	0.60
	0.05	−0.35	7.00E−07	0.0080	0.60	0.60
	0.70	−0.35	7.00E−07	0.0080	0.60	0.05
	3.50	−0.35	7.00E−07	0.0080	0.60	0.05
LDX 2003	0	−0.34	5.00E−07	0.0059	0.60	0.60
	0.05	−0.35	5.00E−07	0.0059	0.62	0.62
	0.70	−0.35	6.00E−07	0.0071	0.65	0.60
	3.50	−0.40	6.00E−07	0.0071	0.60	0.60

pitting corrosion for these concentrations. E_{pit} and E_{rep} for LDX 2003 are not affected by the concentration of chlorides and this alloy always shows negative hysteresis.

3.2 Simulated concrete-pore solution

The affects on the impedance for the three different materials with different ratios of $[Cl^-]/[OH^-]$ around the OCP are represented by the Nyquist diagrams shown in Fig. 6.

As well as in the simulated concrete solution, the EIS signal at OCP was not very different for the three materials in the different chloride concentrations; however, much larger impedance was shown in the tests for LDX 2003. Increasing the $[Cl^-]/[OH^-]$ ratio does not change the signal of the impedance at OCP. The reasons for this are the same as in the simulated concrete solution: the high pH produces a semi-passivation, but there is no formation of a stable passive layer due to the lack of oxygen in the solution.

The effect of increasing the concentration of chloride ions is again evident in the potentiodynamic plots shown in Fig. 7.

In the absence of chlorides, C1008 steel shows a passivation current and potential range similar to those of SS 316L and LDX 2003 alloys, in addition to negative hysteresis, which indicates that pitting corrosion is not likely. The former behavior is also shown when increasing the ratio $[Cl^-]/[OH^-]$ to 0.1. However, when increasing the $[Cl^-]/[OH^-]$ ratio to 1.0, the C1008 steel showed a large positive hysteresis, indicating a likelihood of forming pitting corrosion, and the E_{rep} was lower than the corrosion potential, which indicates more severe corrosion. There is indeed a critical threshold value between $[Cl^-]/[OH^-] = 0.1$ and $[Cl^-]/[OH^-] = 1.0$ for C1008. For the ratio $Cl^-/OH^- = 1.0$, the SS 316L and LDX 2003 alloys showed a behavior similar to what they showed at lower chloride concentrations. Finally, when increasing the $[Cl^-]/[OH^-]$ ratio to 10, the C1008 steel showed the highest current and a positive hysteresis; the SS 316L showed the same passivation current as in lower chloride

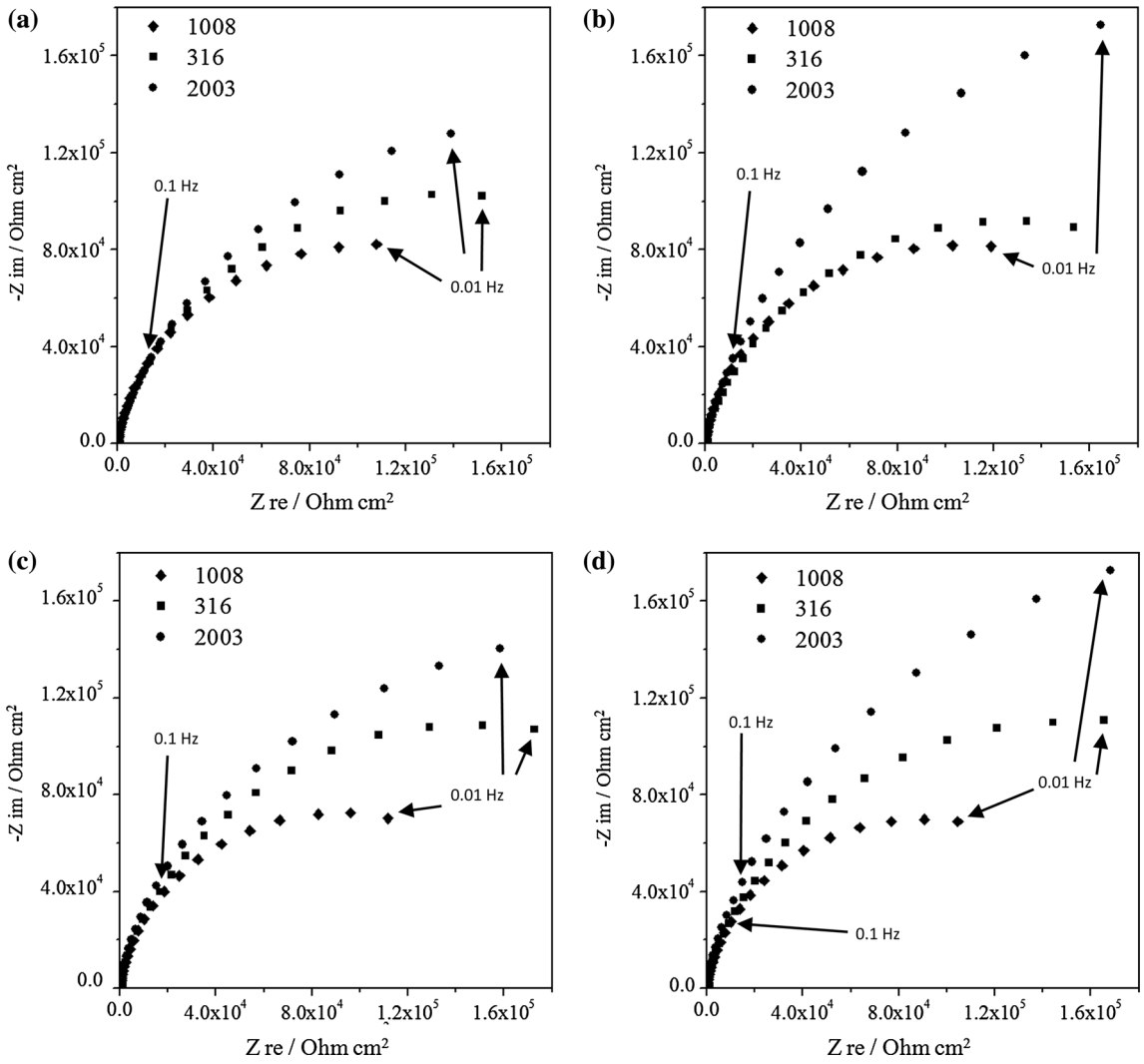

Fig. 6 Nyquist plots for 1,008, 316L, and LDX 2003 in simulated pore solution for the ratios Cl^-/OH^- **a** 0, **b** 0.1, **c** 1.0, and **d** 10

concentrations, but in this case, it also showed positive hysteresis, indicating a likelihood of pitting corrosion. The alloy LDX 2003 showed negative hysteresis at the highest chloride concentration and an E_{rep} similar to that in the simulated concrete solution. This alloy thus showed negative hysteresis in both the simulated concrete solution and the simulated concrete-pore solution, as well as similar E_{rep} values. The damage caused by pitting in the SS 316L alloy at a ratio $[Cl^-]/[OH^-] = 10$ and the resistance of the LDX 2003 alloy to this damage can be observed in the SEM images in Fig. 8 and the 3D micrograph in Fig. 9.

Table 3 shows the corrosion parameters obtained from the potentiodynamic experiments in the concrete-pore simulated solution. As well as in the concrete simulated solution experiments, E_{corr} is very similar for all the materials in the different chloride concentrations, J_{corr} and V_{corr} are also quite similar except for the case of low-carbon steel. C1018 steel shows a $[Cl^-]/[OH^-]$ threshold value between 1.0 and 10.0 for the corrosion rate parameter, however, for E_{pit} and E_{rep}, this threshold value lies below the ratio of 1.0. Even though E_{pit} also shows a threshold value above 1.0, dropping 800 mV for the ratio of 10, E_{rep} shows a threshold value below the ratio of 1.0 crossing the reverse scan below E_{corr} with positive hysteresis; these results indicate that the likelihood of having pitting corrosion is high below the $[Cl^-]/[OH^-]$ ratio of 1.0. For SS 316L, E_{pit} remains constant and it is not affected by the concentration of chlorides, however, E_{rep} drops 600 mV from E_{pit} with a positive hysteresis for the ratio of 10.0, indicating the likelihood of pitting corrosion in this concentration. E_{pit} and E_{rep} for LDX 2003 are not affected by the concentration of chlorides and this alloy always shows negative hysteresis.

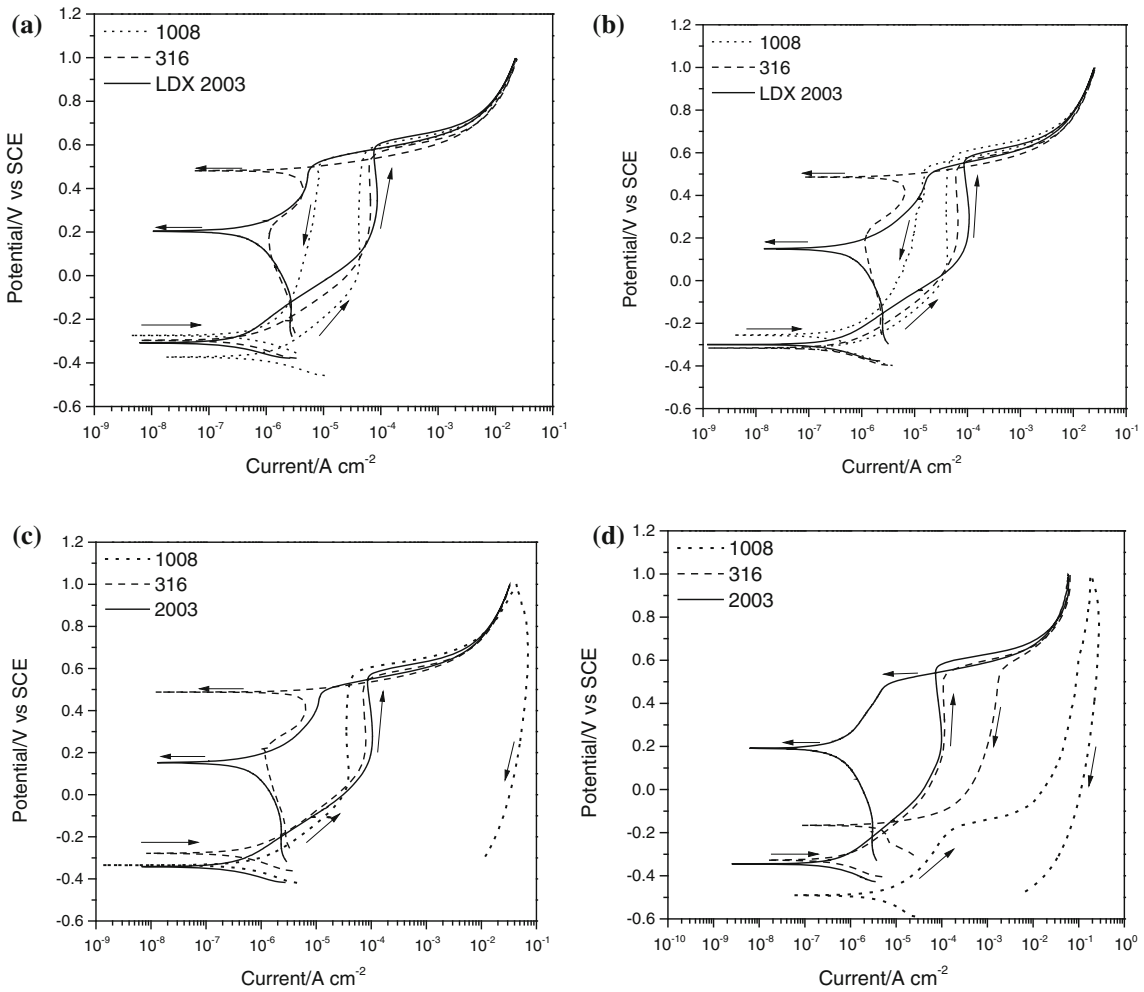

Fig. 7 Potentiodynamic plots for 1,008, 316L, and LDX 2003 in simulated concrete-pore solution for Cl^-/OH^- ratios **a** 0, **b** 0.1, **c** 1.0, and **d** 10; all the sweep rates were 1 mV s^{-1}

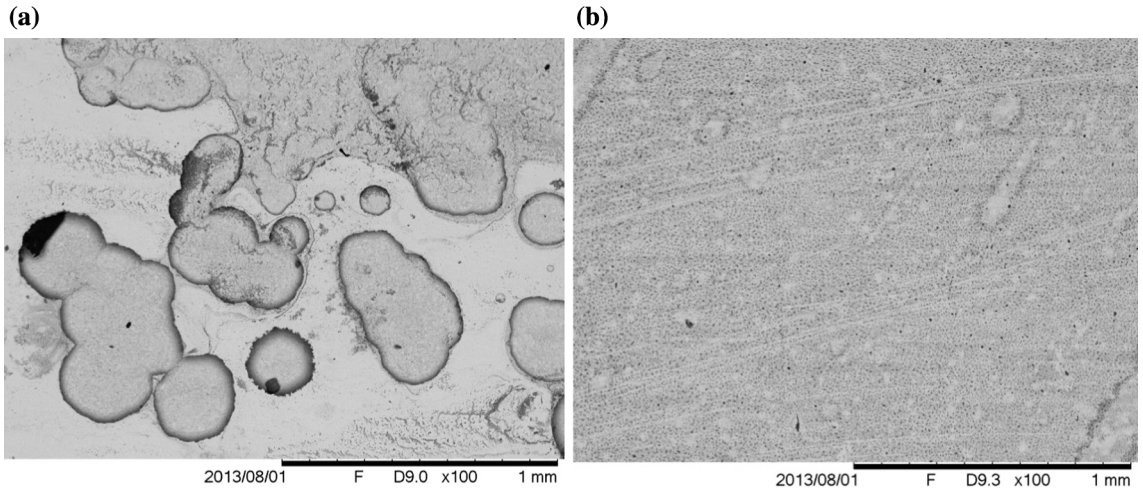

Fig. 8 SEM images for simulated concrete-pore solution exposed to a ratio of $Cl^-/OH^- = 10$ for **a** pits on 316 L at ×100, **b** no damage on LDX 2003 at ×100

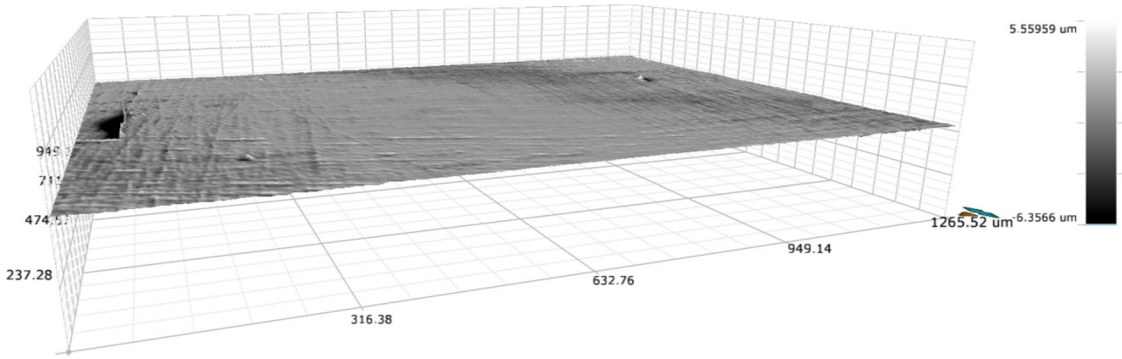

Fig. 9 3D Optical micrograph for LDX 2003 in simulated concrete-pore solution with a ratio $Cl^-/OH^- = 10$; no pits or damages were found on the surface

Table 3 Corrosion parameters for concrete-pore simulated conditions

Alloy	Cl^-/OH^-	E_{corr} ($V_{vs\ SCE}$)	J_{corr} (A cm^{-2})	V_{corr} (mm y^{-1})	E_{pit} (V_{vsSCE})	E_{rep} (V_{vsSCE})
C1008	0	−0.38	2.00E−06	0.0233	0.60	0.58
	0.10	−0.30	1.00E−06	0.0116	0.60	0.55
	1.00	−0.31	2.00E−05	0.0174	0.60	–
	10.0	−0.48	8.00E−07	0.2330	−0.20	–
SS 316L	0	−0.30	3.00E−07	0.0034	0.55	0.53
	0.10	−0.32	1.00E−06	0.0114	0.58	0.55
	1.00	−0.28	1.00E−06	0.0114	0.55	0.53
	10.0	−0.32	1.00E−06	0.0114	0.55	−0.15
LDX 2003	0	−0.30	2.00E−07	0.0023	0.60	0.60
	0.10	−0.30	2.00E−07	0.0024	0.60	0.55
	1.00	−0.33	3.00E−07	0.0035	0.60	0.55
	10.0	−0.33	3.00E−07	0.0024	0.58	0.54

3.3 Potentiostatic tests for LDX 2003 in simulated concrete solution

EIS spectra were obtained, while applying an anodic overpotential of 0.04 V versus Ref under two conditions: without chlorides and with 3.5 wt% of NaCl; this overpotential was carefully selected to account for the beginning of the passive region for the LDX 2003 alloy. AFM was used to analyze the growth of corrosion products and the surface modification. EIS was performed at three different times: at the beginning of the test, after 5, and 11 h after initiating the test; this allowed the alloy to start forming the passive layer seen in the potentiodynamic plots. Figure 10 shows the EIS spectra for these different times in the absence of chloride ions.

In the EIS spectra of Fig. 10, it is possible to see the evolution of the interface from the beginning of the test to the 11th h; the magnitude of the impedance becomes larger, which indicates the growth of a passive layer under the experimental conditions. The surface analysis for the layer evolution using AFM and 3D optical microscopy was carried out as a comparison between the initial state and at the end of the 11 h; this is shown in Figs. 11 and 12.

The changes on the surface shown in Figs. 11 and 12 are no significant, and they only show the growth of corrosion products or perhaps the precipitation of various species; the only effect of polarizing was to grow the passive film on the surface. Figure 13 shows the impedance diagrams for LDX 2003 in simulated concrete solution with the addition of 3.5 wt% NaCl and an anodic overpotential of 0.04 V versus Ref. In the complex diagram, it is possible to observe a remarkable difference between the system at the beginning of the test and after prolonged exposure to the solution. In the initial stage, the impedance is shorter in magnitude, hence the charge transfer resistance (R_{ct}) is much less than at later times; this difference is indicative of high activity in the presence of chloride ions during the initial time period, and it is much more evident in the phase diagram. In this diagram, each different times has two constants, since the formation and growth of a protective

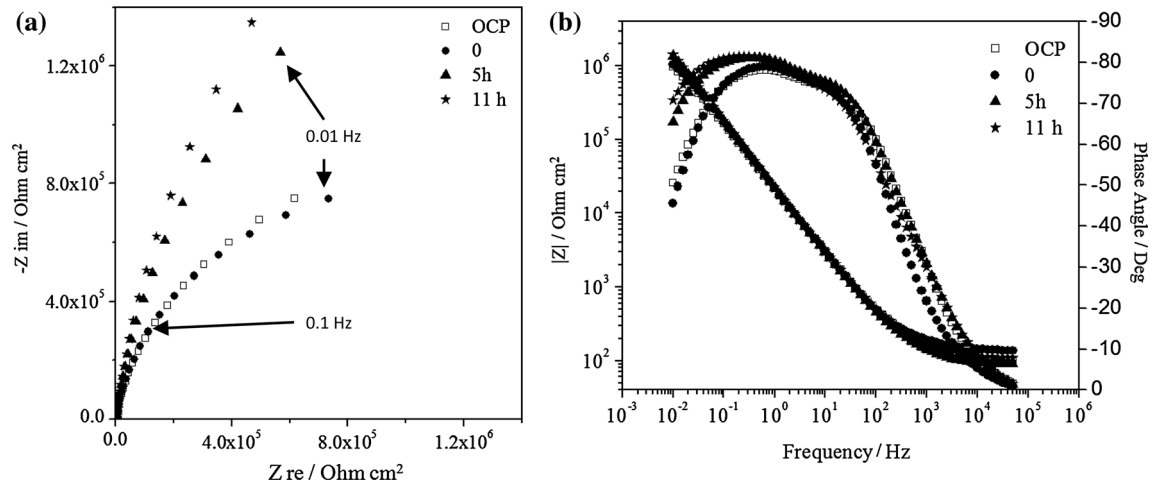

Fig. 10 Nyquist (**a**) and Bode (**b**) plots for LDX 2003 in 2 g L^{-1} $Ca(OH)_2$ without chloride ions. EIS carried out at an applied potential of 0.04 V versus Ref at different times

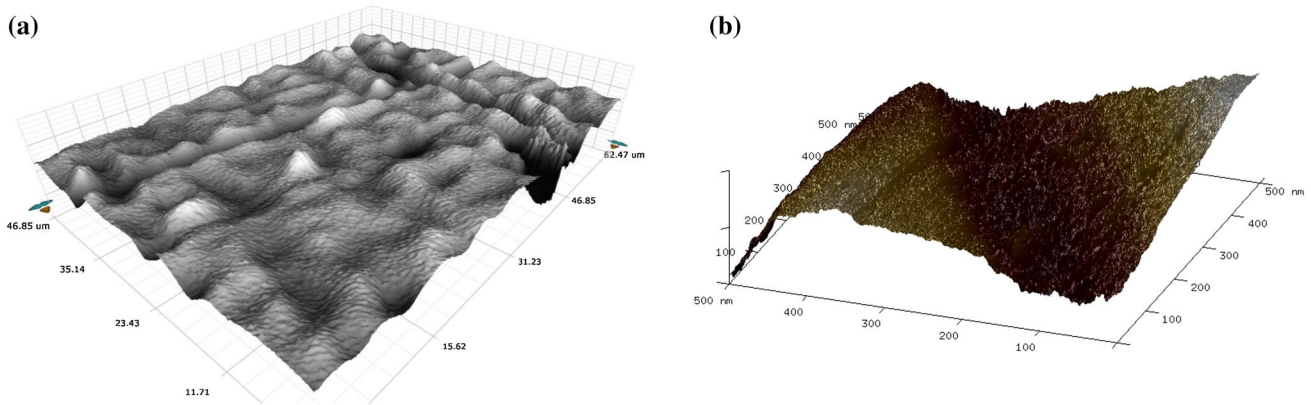

Fig. 11 LDX 2003 at the beginning of the test **a** 3D microscopy, ×100, Ra = 27.547 nm, and **b** AFM Ra = 5.28 nm

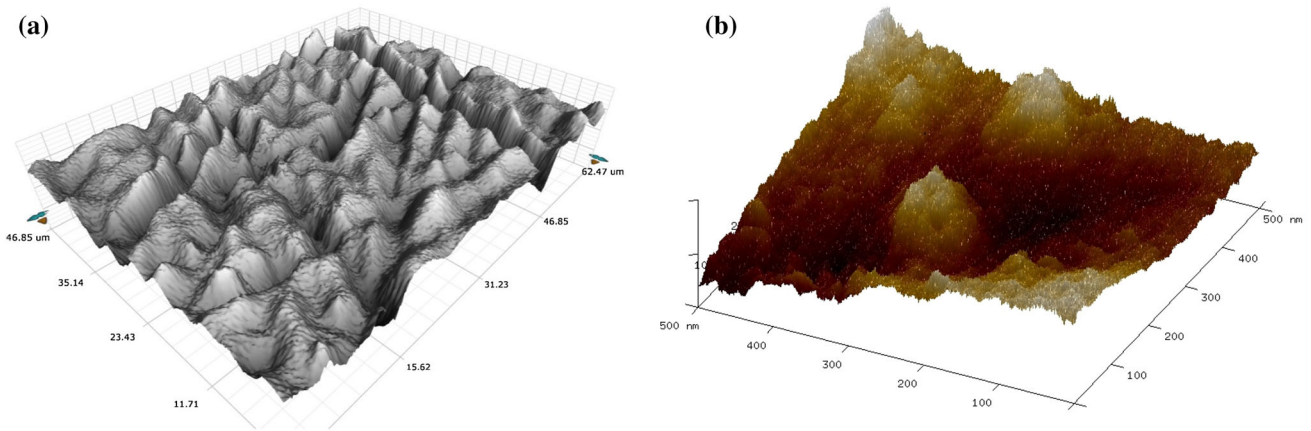

Fig. 12 LDX 2003 after 11 h of exposure to a 2 g L^{-1} $Ca(OH)_2$ solution and an anodic overpotential of 300 mV **a** 3D microscopy, ×100, Ra = 34.351 nm, and **b** AFM Ra = 2.92 nm

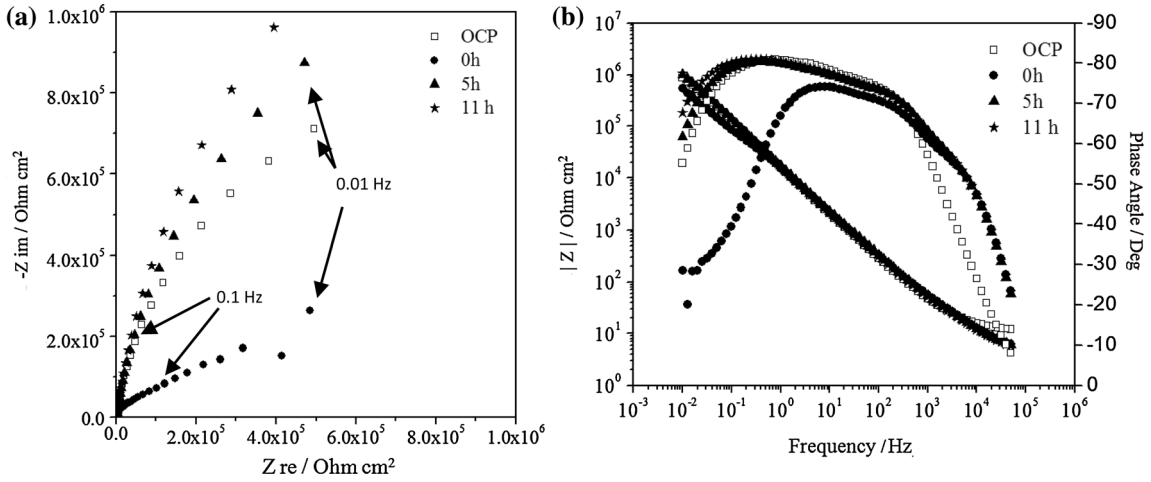

Fig. 13 Evolution of the electrochemical signal in function of time for LDX 2003 in 2 g L^{-1} $Ca(OH)_2$ + 3.5 wt% NaCl at E applied = 0.04 V versus Ref. **a** Nyquist plot, and **b** Bode plot

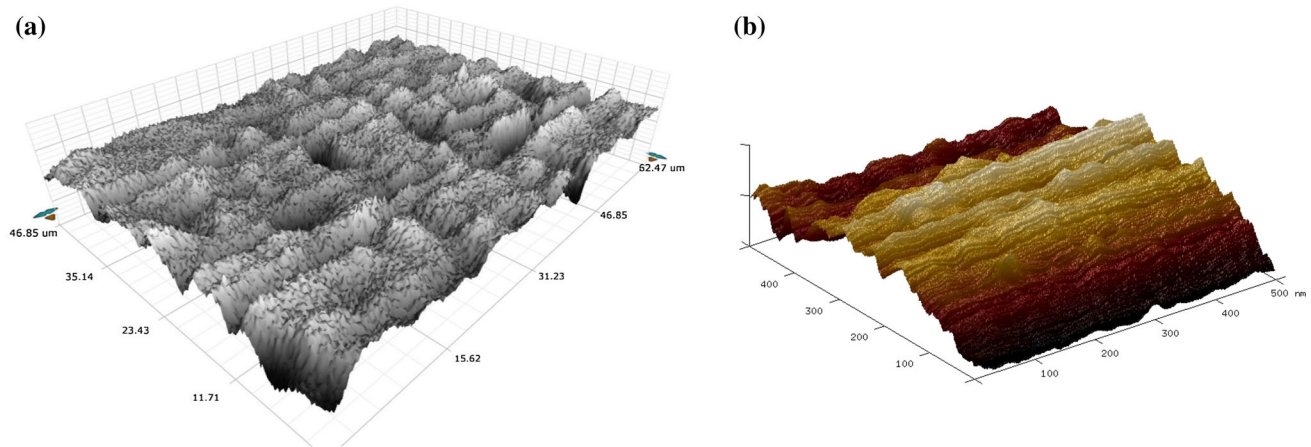

Fig. 14 LDX 2003 **a** 3D micrograph, ×100 Ra = 25.92 nm, and **b** AFM before exposure to 2 g L^{-1} $Ca(OH)_2$ + 3.5 wt% NaCl, Ra = 2.26 nm

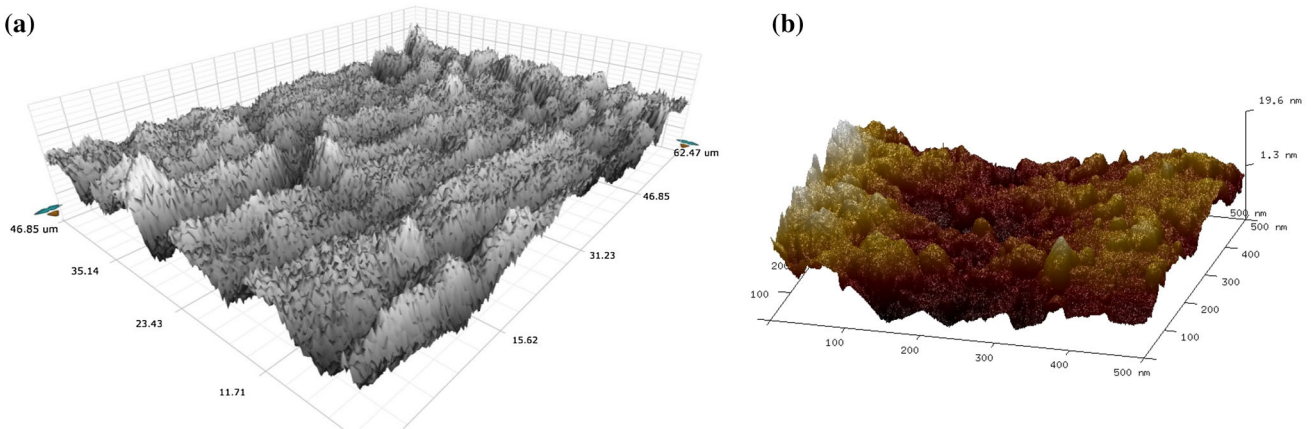

Fig. 15 LDX 2003 after 11 h of exposure **a** 3D micrograph, ×100, Ra = 21.053 nm, and **b** AFM Ra = 4.29 nm after exposure to solution and an anodic overpotential of 300 mV, 2 g L^{-1} $Ca(OH)_2$ + 3.5 wt% NaCl

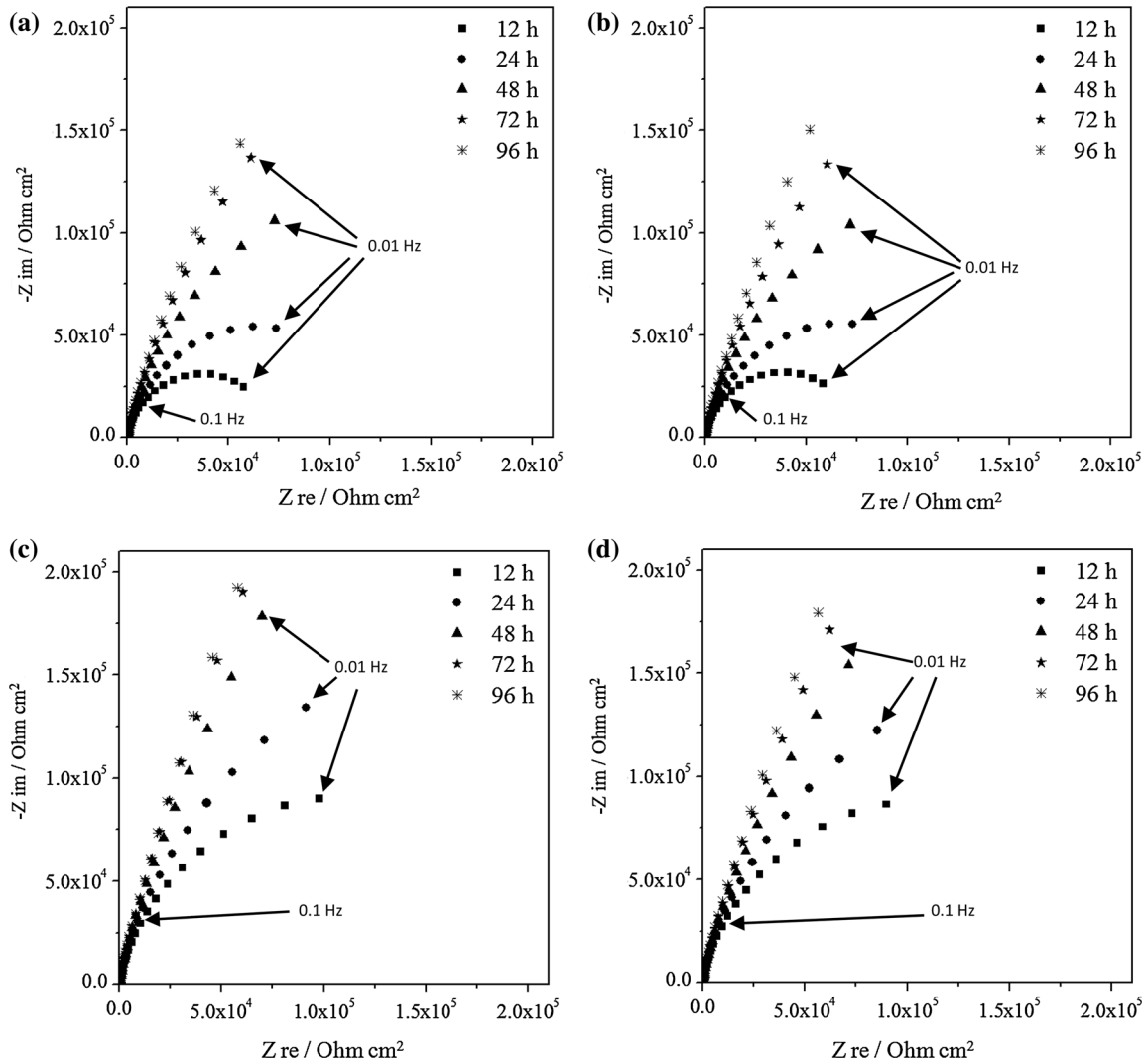

Fig. 16 Nyquist plots as functions of time for LDX 2003 in simulated concrete-pore solution with Cl^-/OH^- ratios of **a** 0, **b** 0.1, **c** 1.0, and **d** 10

oxide layer happens even in the presence of chloride ions. In summary, the effect of the chloride ions is only evident during the initial stages, and then it is almost immediately hidden by the formation of a protective passive film.

As in the case without chlorides, Figs. 14 and 15 show a comparison of the LDX 2003 alloy before and after being exposed to the chloride environment. Figure 14 shows the 3D micrograph and the AFM images before the test, and Fig. 15 shows the images for the sample in the simulated concrete solution with the addition of 3.5 wt% of NaCl after 11 h of an anodic overpotential of 0.04 V versus Ref.

The differences in the surface before and after the experimental conditions shown in Figs. 14 and 15 are barely distinguishable. As in the EIS plots, the differences are minimal, and the summary for these two systems is that there is no effect of the chloride ions once the protective passive film has developed.

3.4 Potentiostatic tests for LDX 2003 in simulated concrete-pore solution

Potentiostatic tests were carried out for the LDX 2003 that allows a passivation potential of 600 mV versus OCP was applied for 96 h until a steady state current was reached. EIS was carried out every 12 h to determine if the impedance indicated the passivation behavior. Selected impedance spectra are shown in Figs. 16 and 17, and the surface as observed by a 3D microscope is shown in Fig. 18.

Figures 16 and 17 show the impedance signal corresponding to the evolution of the passive film on the LDX 2003 alloy from hour 12 to hour 96. In Fig. 16, it is noticeable that the signal changed from an active (charge transfer) behavior (an incomplete semicircle) to a passive or capacitive behavior (a straight line) with high values of

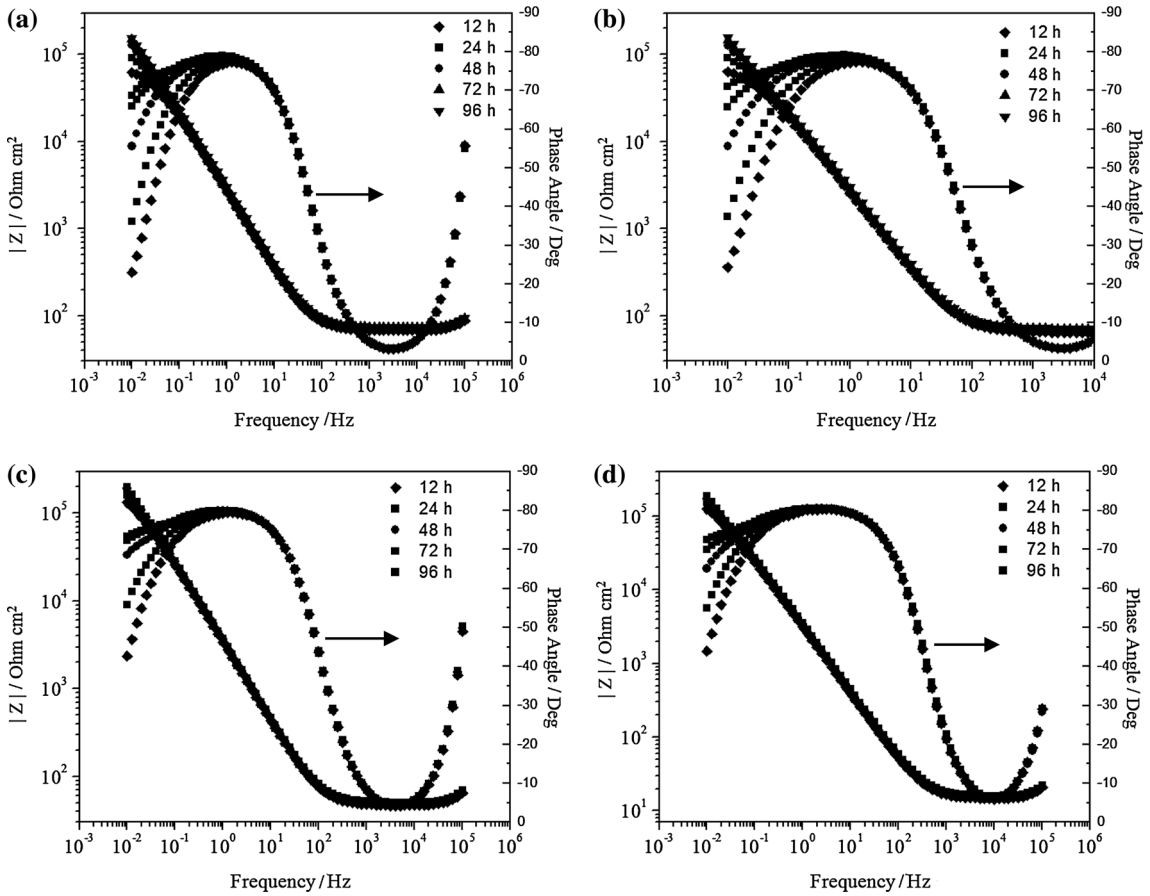

Fig. 17 Bode plots as functions of time for LDX 2003 in simulated concrete-pore solution with Cl^-/OH^- ratios of **a** 0, **b** 0.1, **c** 1.0, and **d** 10

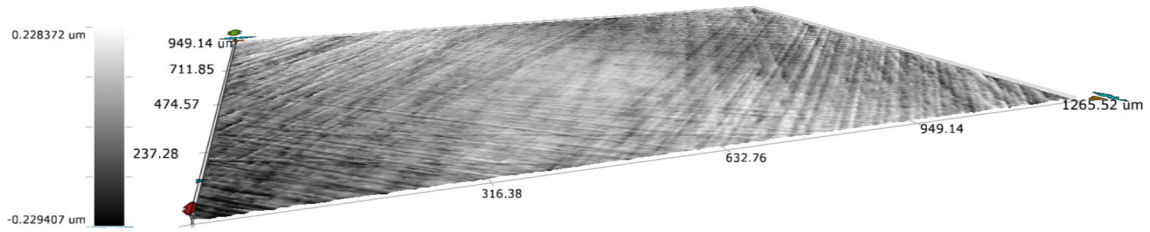

Fig. 18 3D Optical micrograph for LDX 2003 in simulated concrete-pore solution with $Cl^-/OH^- = 10$, after being polarized at 600 mV versus OCP during 96 h; no damage was observed

impedance (high R_{ct}). In the Bode plots of Fig. 17, the only visible change is an increase in the angle at lower frequencies, which is only due to an increase in the resistance of the layer. Since there is no oxygen present in the solution, the layer takes longer to achieve stability, and the effect of this is an increase in the resistance of the interface.

As it can be observed in Fig. 18, the LDX 2003 alloy shows no damage by pitting and the surface is smother than in the cases when the sample was polarized with 1.0 V; the range between the lowest and the highest points on the surface is 0.5 μm. In order to follow the evolution of the interface as a function of time and the effect of the chloride ions on the performance of LDX 2003, the experimental results were fitted using an equivalent electrical circuit with a resistance simulating the resistance of the electrolyte (R_s) in series with a circuit in parallel containing the R_{ct} and a constant phase element. The interfacial capacitance was calculated based on the derivation by Hirschorn et al. [23]. The results of the fitting per unit area are shown in Table 4.

As can be observed in Table 4, the solution resistance changes accordingly to the conductivity of the solution; the more chloride ions in solution, the less the R_s. Regarding the evolution of the interface, we observe that the capacitive behavior of the interface changes neither with time nor

Table 4 Parameters from the model at different $[Cl^-]/[OH^-]$ ratios and times

Cl^-/OH^- ratio	Time (h)	R_s (Ohm)	R_{ct} (Ohm)	Ceff/10e-5 (F)
0	24	13.03	22100	3.09
0	48	12.59	45,800	2.75
0	72	11.68	75,000	2.51
0	96	11.80	94,050	2.48
0.1	24	12.48	22,457	3.14
0.1	48	12.10	44,465	2.73
0.1	72	11.33	72,383	2.58
0.1	96	11.44	112,519	2.45
1.0	24	9.19	60,442	2.19
1.0	48	8.82	116,976	2.07
1.0	72	8.20	150,139	2.03
1.0	96	8.20	169,654	2.05
10.0	24	2.95	54,805	2.04
10.0	48	2.80	86,653	1.96
10.0	72	2.57	112,892	1.88
10.0	96	2.57	142,758	1.63

with an increase in the chloride concentration; the value for the capacitance remains stable, which indicates a stable interface not affected by the presence of chloride. The R_{ct} increases with time, but it is not affected by the presence of chloride ions, the magnitudes at the different concentrations are similar and the changes in time are due to the stability (growth) of the passive layer on the surface. The stability of the capacitance and R_{ct}, independent of the concentration of chloride ions, can be better observed in Fig. 19.

It is clear from Fig. 19 that the passive layer has not yet reached stability, since the R_{ct} continues growing and the capacitance continues decreasing as a function of time. For a fully developed and stable passive film we would expect these values to be constant. The important feature shown in this plot is that the tendency of the R_{ct} to increase and the capacitance to decrease is the same regardless of the concentration of chlorides. Also, the magnitude of those values is in a very narrow range, and thus, it demonstrates that this specific environment does not affect the LDX 2003 alloy.

The main differences on the behavior shown between the different alloys are the passive film formed on the surface; this film formation follows different corrosion mechanism. The corrosion mechanism for carbon steel is recognized to be different when it is time dependent than when it is potential dependent; when the mechanism is function of time, reactions 1–4 are accepted [12, 24]:

$$Fe \rightarrow Fe^{2+} + 2e^- \quad (1)$$

$$Fe^{2+} + 2H_2O \rightarrow Fe(OH)_2 + 2H^+ \quad (2)$$

$$3Fe(OH)_2 + 2OH^- \rightarrow Fe_3O_4 + 4H_2O + 2e^- \quad (3)$$

and when the mechanism is function of potential, one more reaction occurs [12, 24]:

$$Fe_3O_4 + OH^- + H_2O \rightarrow 3FeOOH + e^- \quad (4)$$

In corrosion resistant alloys such as stainless steels and lean duplex, the mechanism does not involve the release of iron ions to form the passive film, but instead, the formation of a chromium oxide inner layer and an iron oxide outer layer [6, 12, 13, 17]. The reason for the high corrosion resistance and the high pitting corrosion resistance of stainless steel and lean-duplex steel are the presence of molybdenum and nitrogen in the lean duplex. It has been demonstrated that molybdenum, as MoO_4^{2-}, creates ionic

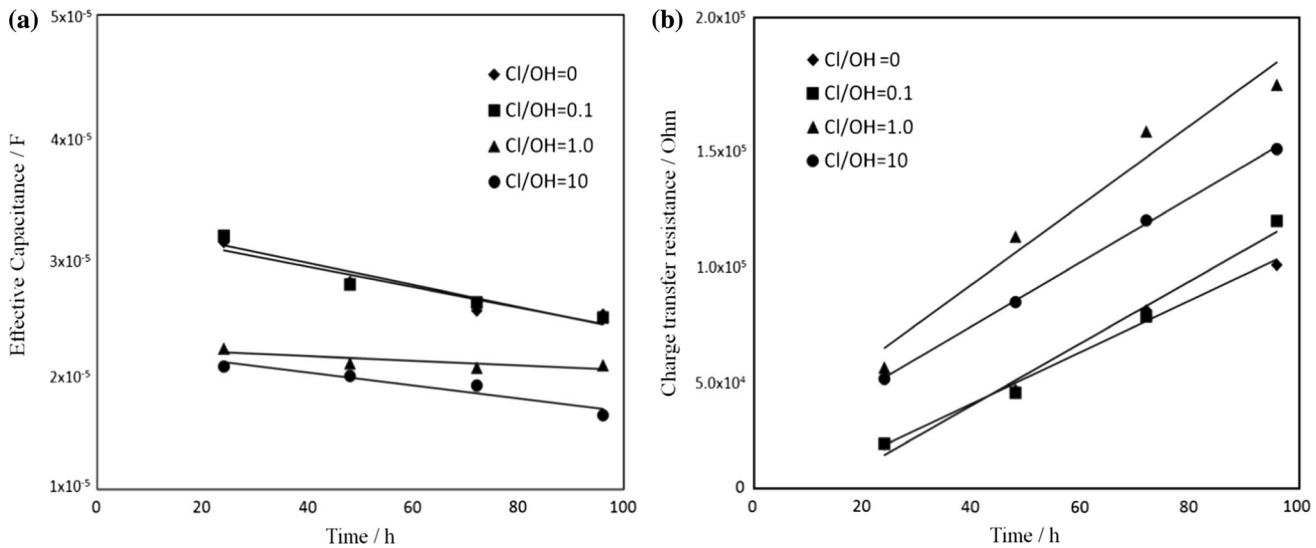

Fig. 19 Values for **a** effective capacitance and **b** R_{ct}, for the different concentrations of chloride ions as a function of time

selectivity to form Cr_2O_3 and CrO_3 and helps to stabilize these species; in addition, it neutralizes the positive donors and decreases the conductivity in the passive film. Molybdenum decreases the p-type acceptors in the Cr-oxide layer and decreases the n-type donors in the Fe-oxide layers [17], and more importantly, it protects the ferrite phase inducing the dissolution of the austenitic phase [6]. Differences between the stainless steel and the lean-duplex steel are the high nitrogen content in the lean-duplex steel; nitrogen has been proven to promote the pit repassivation but not the pit initiation, in addition, the likely formation of chromium and molybdenum nitrides in the bottom of the pit which causes pit repassivation [25, 26].

4 Conclusions

In the simulated concrete solution and simulated concrete-pore solution, the presence of chlorides has no effect on the lean-duplex LDX 2003 and its localized corrosion performance over the low-carbon steel (AISI 1008) and stainless steel (SS 316L) under the same environmental conditions shows better results.

There is no chloride concentration threshold inducing the formation of pitting corrosion in the range used in this work for LDX 2003, chlorides did not cause any damage by pitting.

It is believed that the content of molybdenum and nitrogen induces the corrosion resistance of the ferrite phase and the pit repassivation in the lean-duplex steel, the corrosion attack by the presence of chlorides inducing the pitting corrosion is reduced by the repassivation cause by nitrogen forming nitrides of chromium and molybdenum in the bottom of the pit [25].

EIS performed on LDX 2003, while applying potential in the range of the passive region, showed the evolution of the passive layer from a charge transfer to a capacitive behavior indicating the development of a passive film in function of time. This film was not affected by the highest concentration of chlorides used in this work (3.5 wt% NaCl).

Acknowledgments This work is associated with the Corrosion Program at The University of Akron. We acknowledge the support of the Construction Engineering Research Laboratory (CERL), US Department of Defense Office of Corrosion Policy and Oversight.

References

1. Roberge PR (2012) Handbook of corrosion engineering, 2nd edn. McGraw-Hill, New York, p 1078
2. Ye CQ et al (2013) EIS analysis on chloride-induced corrosion behavior of reinforcement steel in simulated carbonated concrete pore solutions. J Electroanal Chem 688:275–281
3. Fajardo S et al (2010) Low-nickel stainless steel passive film in simulated concrete pore solution: a SIMS study. Appl Surf Sci 256(21):6139–6143
4. Veleva L et al (2005) Voltammetry and surface analysis of AISI 316 stainless steel in chloride-containing simulated concrete pore environment. J Electroanal Chem 578(1):45–53
5. Feng X, Tang Y, Zuo Y (2011) Influence of stress on passive behaviour of steel bars in concrete pore solution. Corros Sci 53(4):1304–1311
6. Freire L et al (2011) The electrochemical behaviour of stainless steel AISI 304 in alkaline solutions with different pH in the presence of chlorides. Electrochim Acta 56(14):5280–5289
7. Abreu CM et al (2006) Long-term behaviour of AISI 304L passive layer in chloride containing medium. Electrochim Acta 51(8–9):1881–1890
8. Valcarce MB, López C, Vázquez M (2012) The role of chloride, nitrite and carbonate ions on carbon steel passivity studied in simulating concrete pore solutions. J Electrochem Soc 159(5):C244–C251
9. Paredes EC et al (2012) Influence of the forming process of corrugated stainless steels on their corrosion behaviour in simulated pore solutions. Corros Sci 58:52–61
10. Blanco G, Bautista A, Takenouti H (2006) EIS study of passivation of austenitic and duplex stainless steels reinforcements in simulated pore solutions. Cement Concrete Compos 28(3):212–219
11. Alvarez SM, Bautista A, Velasco F (2011) Corrosion behaviour of corrugated lean duplex stainless steels in simulated concrete pore solutions. Corros Sci 53(5):1748–1755
12. Freire L et al (2012) Electrochemical and analytical investigation of passive films formed on stainless steels in alkaline media. Cement Concrete Compos 34(9):1075–1081
13. Elsener B et al (2011) Stainless steel reinforcing bars—reason for their high pitting corrosion resistance. Mater Corros 62(2):111–119
14. Mesquita TJ et al (2011) Anomalous corrosion resistance behavior of Mo-containing SS in alkaline media: the role of microstructure. Mater Chem Phys 126(3):602–606
15. Mesquita TJ et al (2012) Lean duplex stainless steels—the role of molybdenum in pitting corrosion of concrete reinforcement studied with industrial and laboratory castings. Mater Chem Phys 132(2–3):967–972
16. Abreu CM et al (2004) Comparative study of passive films of different stainless steels developed on alkaline medium. Electrochim Acta 49(17–18):3049–3056
17. Montemor MF et al (1999) The role of Mo in the chemical composition and semiconductive behaviour of oxide films formed on stainless steels. Corros Sci 41(1):17–34
18. Luo H et al (2012) The electrochemical behaviour of 2205 duplex stainless steel in alkaline solutions with different pH in the presence of chloride. Electrochim Acta 64:211–220
19. Gao J et al (2009) Investigation of selective corrosion resistance of aged lean duplex stainless steel 2101 by non-destructive electrochemical techniques. Electrochim Acta 54(24):5830–5835
20. Dunn JJ, Hasek DR, Clements R (2007) AL 2003^{TM} (S232003) lean duplex case study: flexible flowlines for an offshore oil field development. In: Stainless steel world conference 2007. KCI Publishing bv, The Netherlands
21. Charlse JCP (2010) The history of duplex developments, nowadays DSS properties and duplex market future trends. In: 8th Duplex stainles steels conference. Beaune, France
22. Frankel GS (1998) Pitting corrosion of metals: a review of the critical factors. J Electrochem Soc 145(6):2186–2198
23. Hirschorn B et al (2010) Determination of effective capacitance and film thickness from constant-phase-element parameters. Electrochim Acta 55(21):6218–6227

24. Sánchez M et al (2007) Electrochemical impedance spectroscopy for studying passive layers on steel rebars immersed in alkaline solutions simulating concrete pores. Electrochim Acta 52(27):7634–7641
25. Giordano EJ et al (2010) Electrochemical behavior of two austenitic stainless steel biomaterials. Rem Revista Escola de Minas 63:159–166
26. Lim YS et al (2001) The influences of microstructure and nitrogen alloying on pitting corrosion of type 316L and 20 wt% Mn-substituted type 316L stainless steels. Corros Sci 43(1):53–68